Available online at www.sciencedirect.com
SCIENCE DIRECT®
Journal of Power Sources 124 (2003) 133–142
JOURNAL OF POWER SOURCES
www.elsevier.com/locate/jpowsour

Self-assembled monolayers of diphenyl disulphide: a novel cathode material for rechargeable lithium batteries

Trupti Maddanimath, Yogesh B. Khollam, M. Aslam, I.S. Mulla, K. Vijayamohanan*

Physical and Materials Chemistry Division, National chemical Laboratory, Dr. Homi Bhabha Road, Pune 411008, India

Received 18 March 2003; accepted 5 May 2003

Abstract

The use of self-assembled monolayers (SAM) of organic disulfide as novel cathode materials for high specific energy, rechargeable, lithium batteries is demonstrated for the first time. The suitability of monolayer films of diphenyl disulfide (DDS) as cathode materials for facilitating reversible insertion and de-insertion of Li^+ ions is examined by means of cyclic voltammetry (CV), infra-red spectroscopy (FTIR), X-ray photoelectron spectroscopy (XPS), and charge–discharge measurements. The SAM-based cathodes on coupling with Li-metal anodes in 0.1 M $LiClO_4$ and tetrahydrofuran (THF) show good thermodynamic feasibility along with an open-circuit voltage of 2.9 V. The electrochemical capacity obtained is found, however, to fade during continuous cycling. This indicates a loss of electroactivity concomitant with the destruction of the monolayer functionalized cathode. The reasons for the coulombic efficiency of these rechargeable SAM-based cathodes are explained in terms of two different mechanistic modes of interaction of Li^+ ions with the monomolecular film.

Keywords: Self-assembled monolayer; Diphenyl disulfide; Cathode material; Rechargeable lithium battery; Coulombic efficiency; Capacity

1. Introduction

Rechargeable lithium batteries are attractive power sources because of their high specific energy/power and long operational life compared with other rechargeable batteries [1,2]. Consequently, lithium batteries are used routinely in several electronic devices that include laptop computers, cellular phones, electronic watches, calculators, cameras, oxide semiconductor memories, electric vehicles, and human inplantable devices. In these applications, light weight and the small size are the crucial aspects for optimizing the device performance [1–4]. Although different types of rechargeable lithium cathodes such as transition metal oxides [5–7], organic compounds [8], chalcogenides [9], and complex metal oxides [10] are presently commercially available, their performance does not meet all the goals required for the development of batteries with efficient high specific powers [11]. Conventional cathode materials [12–14] also exhibit several drawbacks, such as: (i) a low capacity at moderate current density, surface degradation and grain growth during both cycling and in open-circuit stand; (ii) a high rate of self-discharge due to parasitic corrosion reactions; (iii) a large Ohmic drop due to the formation of insulating phases [11,15]. Further, problems like poor mechanical strength, poor utilization efficiency, relatively slow transfer of Li^+ ions and large Ohmic drop arise due to the use of external additives such as graphite or acetylene black and also polymeric binders during the cathode fabrication. Recently, conducting polymer-based cathode materials, which include several organo-inorganic nanocomposites, have been found to be promising to alleviate some of these difficulties so that high specific energy and improved cycle-life can be obtained. Sotomura and co-workers [2] have shown the potential use of 2,5-dimercapto-1,3,4-thiadiazole (DMcT) as a part of composite cathode material for rechargeable lithium batteries, where thiol/disulfide redox processes facilitate the transfer of lithium ions. Most of such materials still, however, show capacity failure during continuous cycling and, more significantly, poor Li^+ transport limits their high-rate capability [16]. Therefore, the development of cheaper, environmentally benign and lightweight rechargeable cathodes which have high specific energy/power and long life still remains a challenge.

Self-assembled monolayers (SAM) are close-packed arrays of amphiphilic molecules like long-chain thiols and disulfides where the high coverage (10^{12} to 10^{13} molecules/cm^2) and monomolecular thickness can be used to design optimum energy/weight or energy/volume parameters. SAM molecules have great freedom and flexibility in their dynamic nature that cause dynamic re-organization. Easy preparation, reproducible film quality, good stability

* Corresponding author. Fax: +91-20-5893044.
E-mail address: viji@ems.ncl.res.in (K. Vijayamohanan).

0378-7753/$ – see front matter © 2003 Elsevier B.V. All rights reserved.
doi:10.1016/S0378-7753(03)00607-4

and control of the chain length to obtain the desired wetting and adhesion properties are the main advantages of the SAM. Due to these reasons, SAM find tremendous applications in various areas such as corrosion protection [17], wetting [18], friction [19], adhesion [20], microelectronics and molecular electronics [21], optics [22], and chemical sensors [23]. The use of these well-ordered monolayers as cathode materials for secondary lithium batteries, despite the possibility of full utilization for a Faradaic reaction, has not been studied. This is perhaps due to the insulating nature of normal SAM forming molecules, e.g. long-chain thiols.

This preliminary study reports the application of diphenyl disulfide (DDS) SAM as a cathode materials for rechargeable lithium batteries. More specifically, a DDS SAM on a copper substrate coupled with a lithium-metal anode in 0.1 M $LiClO_4$/THF as electrolyte is found to undergo reversible intercalation/de-intercalation of lithium ions with an open-circuit voltage (OCV) of 2.9 V. A systematic study of the charge–discharge behaviour using cyclic voltammetry (CV), infra-red spectroscopy (FTIR) and X-ray photoelectron spectroscopy (XPS) has been conducted to understand the insertion/de-insertion mechanism in DDS SAM with respect to the charge storage capacity. DDS is selected on the basis of its well-studied monolayer [24,25] behaviour on different substrates in comparison with long-chain thiols and other disulfides. More interestingly, the presence of a benzene ring can impose a size constraint on the closeness of interlayer packing and hence exert an indirect effect on the mass-transfer characteristics of Li^+ ion insertion. Further, this type of a monolayer-based electrode materials can overcome several limitations that arise due to the use of external additives, e.g. graphite, acetylene black and Teflon binder, during cathode fabrication where the uniformity of mixing, method of electrode fabrication, wetting by electrolyte, etc. play important roles. Lastly, since a monolayer represents the minimum possible amount available on the cathode surface for sustaining an electrochemical reaction, this approach provides an ultimate weight reduction of the active cathode component, which is important in the design of batteries for applications in portable electronics.

Copper has been selected as the main substrate due to its high conductivity, low cost and ease of availability. A few experiments have also been conducted using gold substrates to preclude the active role of copper. Since gold has an affinity towards thiol/disulfides similar to that of copper as well as improved stability of the SAM under ambient conditions (i.e. inert to oxide formation), time-consuming experiments such as charge–discharge measurements have been performed with gold substrates.

2. Experimental

Diphenyl disulfide, lithium perchlorate ($LiClO_4$), and lithium and copper foils (each 99.9%) were purchased from Aldrich chemicals and were used as received. The gold substrates were prepared by the thermal evaporation of 200 nm gold (purity 99.9%) on a Cr-buffer layer (20 nm) which was first deposited on to conventionally clean glass plates [26]. All the solvents were reagent grade and were used without further purification. The copper foils (1 cm^2 area) were polished by SiC abrasive paper followed by etching using phosphoric acid/sulfuric acid solution (130 ml 85% H_3PO_4, 20 ml 97% H_2SO_4, 60 ml H_2O) for removal of oxide impurities present on the surface [27]. Subsequently, the foils were rinsed extensively with acetonitrile and dried prior to monolayer formation by immersion in a 1 mM solution of DDS [25] to obtain a well-organized monomolecular film [25]. The substrates were removed from the DDS solution, washed repeatedly with the solvent, and then dried in a stream of argon. These SAM functionalized copper/gold electrodes as cathodes were coupled with a large-area lithium-metal anodes using 0.1 M $LiClO_4$ in tetrahydrofuran (THF) as an electrolyte to fabricate cells.

Electrochemical charge–discharge measurements were conducted for the initial few cycles using a constant current density of 0.03 mA cm^{-2} that was controlled with the help of a computerized data-acquisition system. All procedures for handling and fabricating the cells were performed in a argon-filled glove box. The water content in the electrolyte was ensure to be less than 50 ppm by Karl–Fisher titrations. The DDS SAM electrodes were characterized both before and after charge–discharge measurements using CV, FTIR and XPS techniques in order to examine for monolayer destruction after electrochemical cycling. Cyclic voltammetry was performed in an oxygen-free atmosphere with a Scanning Potentiostat Model 362 and a Recorder Model RE015 using a three-electrode cell which comprised the monolayer protected copper as the working electrode, a large-area platinum flag counter electrode, and a Ag/Ag^+ (non-aqueous) reference electrode. The FTIR spectra were recorded using a Shimadzu 8201 PC FTIR spectrometer which operated in the reflectance mode. Only for the pure DDS powder, the Nujol mull technique was used. All spectra were taken at 4 cm^{-1} resolution in the range of 400–3500 cm^{-1}.

X-ray photoelectron spectroscopy (XPS) measurements were performed using a VG Scientific ESCA LAB Mk II spectrometer which operated at a pressure better than 10^{-9} Torr using a monochromatic Mg Kα source ($h\nu$ = 1253.6 eV). The calibration of binding energy (BE) was done using the C 1s (BE = 285 eV) value as a reference. All regions, viz. C 1s, S 2p, O 1s, Li 1s and Cu 2p, were measured with 50 eV pass energy.

3. Results and discussion

Earlier studies using a quartz crystal microbalance (QCM), impedance measurement and CV have suggested that DDS forms a stable and compact monolayer with an apparent electrode coverage (θ) of 96% [26,28]. The facile S–S cleavage during monolayer formation was suggested

as on of the main reasons for the enhanced stability of this monolayer compared with other similar organic disulfides [28]. Since voltammetric studies in non-aqueous electrolytes did not give any positive evidence for reductive desorption or any other mode of electric field induced destruction of DDS SAM, it is considered that this SAM can serve as a cathode for rechargeable lithium batteries.

3.1. Charge–discharge measurements

The charge–discharge profiles of a typical lithium cell fabricated using DDS SAM cathodes, measured at a current density of 0.03 mA cm^{-2} at 30 °C for the first (A) and fifth cycle (B) are shown in Fig. 1(a). The open-circuit voltage of the freshly prepared cell is in the range 2.85–2.98 V and this value is found to be invariant with respect to cycling. During discharge, the voltage first drops rapidly to 2.4 V and then decreases slowly to sustain the Faradaic reaction proceeding at a nominal voltage of about 1.4 V. Although the mass-transport limited region in both charging and discharging plots is found to decrease due to cycling, the nature of the plots is similar. For example, step-like features are clearly present in all the discharge plots. These are attributed to re-organization of SAM during Li^+ ion insertion. Similar staging can be seen even if substantially higher current densities (5–10 times more) are used. Since the cathode is a quasi two-dimensional system with pinholes and other defects, bulk phase changes (like staging for amorphous carbonaceous electrodes during lithium ion insertion) are not possible. The most surprising observation is that the

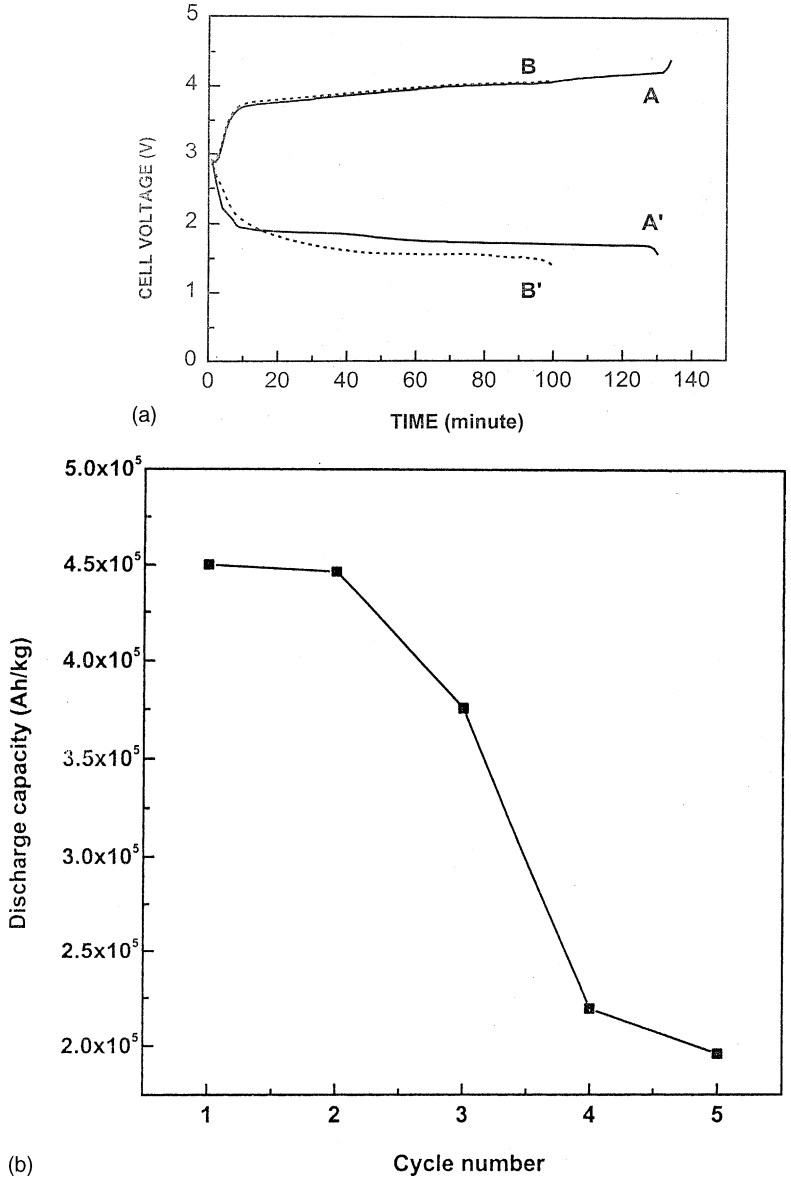

Fig. 1. (a) Charge and discharge profiles for (A, A′) first cycle and (B, B′) fifth cycle of Li-cell consisting of DDS SAM modified Cu as cathode, at rate of 0.03 mA cm^{-2} at 30 °C; electrolyte used is 0.1 M $LiClO_4$ in THF, (b) discharge capacity vs. cycle number.

coulombic capacity is analogous to that of conventional lithium batteries, where the maximum experimental value reported is in the range 400–2000 Ah kg^{-1}, compared with the theoretical value of 3860 Ah kg^{-1} using bulk lithium metal. As the system under consideration is a monomolecular thick monolayer, the conventional capacity calculations for bulk materials are not applicable, hence the average experimental capacity was calculated on the basis of the area of the monolayer. The discharge capacity obtained on the first cycle is around 0.03 mAh cm^{-2}. At a constant current density, the discharge time for accomplishing the same depth-of-discharge (final voltage ~1.4 V) is found to decrease as a function of cycling, as demonstrated in Fig. 1(a). This capacity fading with cycling most likely reflects the limitations of the monolayer stability and can be improved by using more stable disulfide molecules. This variation of capacity as a function of cycle number is shown in Fig. 1(b). Although the capacity for the first two cycles is nearly constant, a 30% decrease is observed on the fifth cycle. In order to evaluate the capacity data obtained for the DDS SAM on copper, charge–discharge measurements were carried out on a gold metal substrate. The charge–discharge profiles for the first five cycles using a SAM functionalized gold electrode as the cathode under similar conditions are presented in Fig. 2. The charge–discharge behaviour corresponds almost exactly to that for a copper substrate (as shown in Fig. 1(a)) but with enhanced capacity. Hence, it can be concluded that the copper reaction may not be responsible for the high coulombic capacity as gold shows similar behaviour. Nevertheless, the reduction in capacity can be avoided by adding a few drops of a millimolar solution of DDS in the electrolyte to effect self-repair of SAM defects. This has been verified by separate experiments.

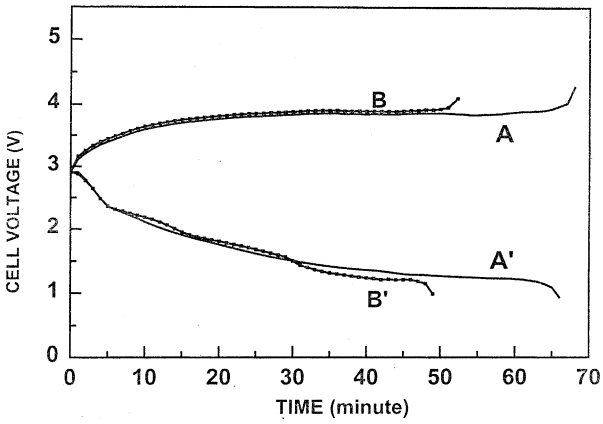

Fig. 2. Charge and discharge profiles for (A, A′) first and (B, B′) fifth cycles of Li-cell consisting of DDS SAM modified Au as cathode, at rate of 0.03 mA cm^{-2} at 30 °C; electrolyte used is 0.1 M $LiClO_4$ in THF.

3.2. Cyclic voltammetry

Superimposed cyclic voltammograms of bare Cu and DDS SAM on copper in 0.1 M $LiClO_4$/THF at a scan rate of 500 mV s^{-1} are shown in Fig. 3(a) and (b), respectively. The drastic reduction in the non-Faradaic current in the case of the voltammogram for the DDS modified copper as compared with that for the bare copper electrode clearly

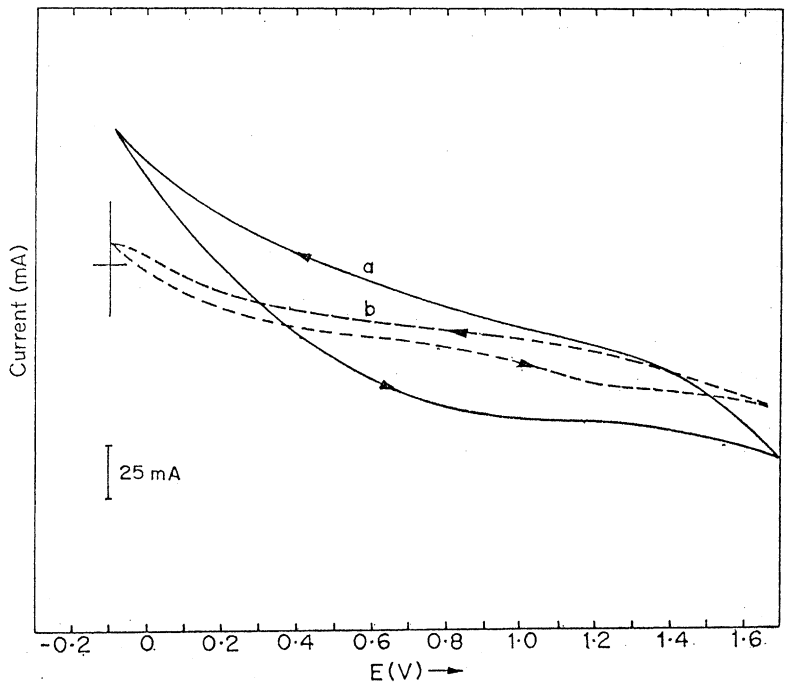

Fig. 3. Superimposed cyclic voltammograms of (a) bare Cu (b) DDS SAM in acetonitrile with 0.1 M $LiClO_4$ as supporting electrolyte and platinum flag as counter electrode at scan rate of 500 mV s^{-1}; vs. Ag/Ag^+ reference electrode.

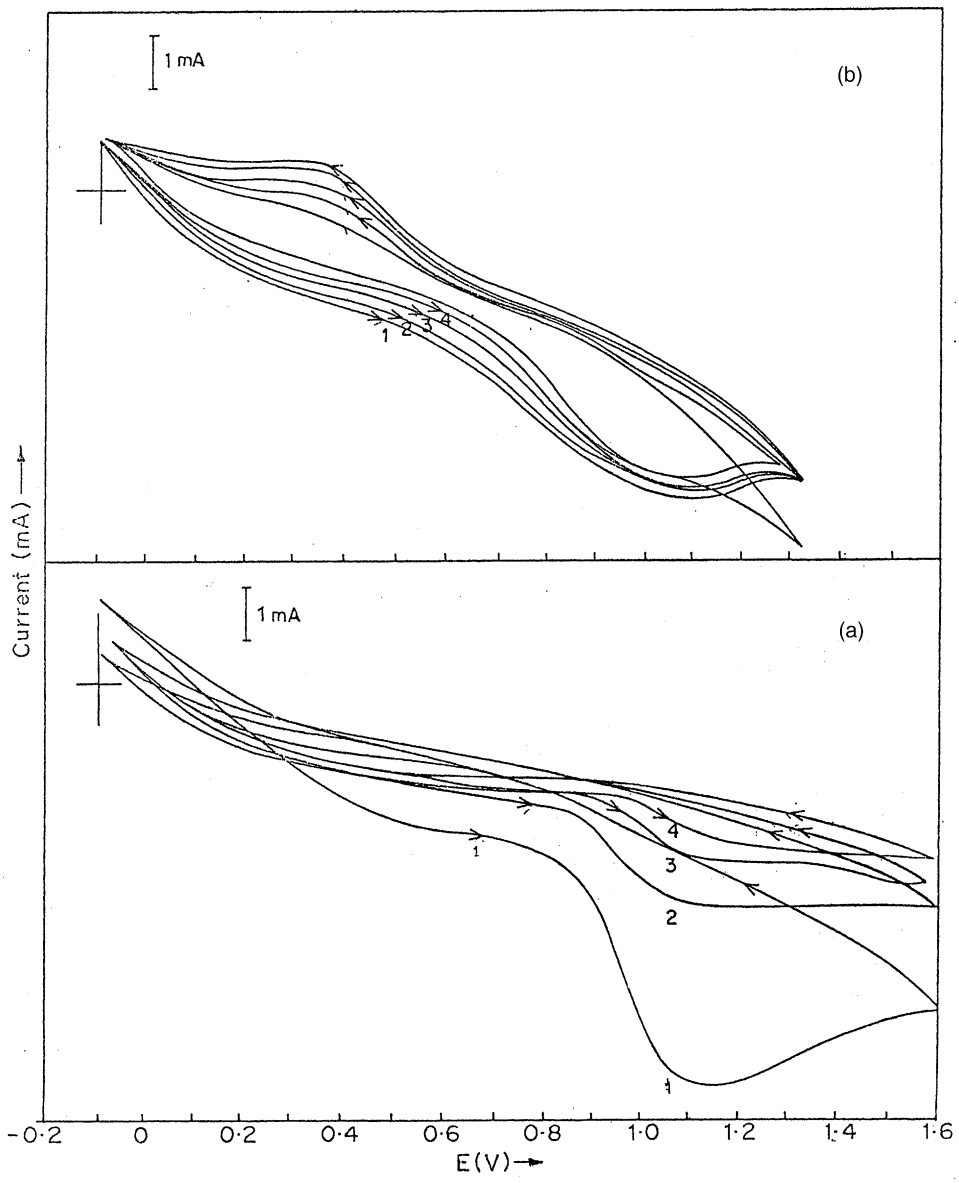

Fig. 4. Cycle dependent voltammograms of (a) discharged DDS SAM and (b) charged DDS SAM at scan rate of 500 mV s^{-1}.

suggests the formation of a compact SAM. In both the cases, no clear redox response is observed, although the raising cathodic current is much larger for the bare copper electrodes. Voltammograms taken for several cycles display identical behaviour. These observations ensure the formation of a well-ordered monolayer on the copper surface, which slows down the electron-transfer kinetics by passivating the surface of copper [25].

The cycle-dependent voltammograms for discharge and charged DDS SAM cathodes are given in Fig. 4(a) and (b), respectively, for the same cycle number in a similar environment. In the discharged sample, a prominent oxidation peak is observed at 1.15 V. Although the peak potential is independent of cycle number, the peak current is seen to diminish considerably with cycling. Since the voltammogram for DDS SAM in the presence of Li^+ ions in the electrolyte (Fig. 3(b)) is electrochemically inert, the above irreversible peak is attributed to the insertion of Li ions which are formed from the lithium-metal anode during the discharge process (Fig. 4(a)). In sharp contrast, the voltammogram for the charged sample gives a quasi-reversible couple with anodic and cathodic peaks at 1.1 and 0.35 V, respectively. This cathodic peak may be attributed to the de-insertion of the Li^+ species present in the charged sample. The oxidation peak (1.1 V) with reduced current indicates the presence of some amount of Li^+ species. This clearly suggests that all the Li ions inserted are not removed by the reverse process and hence accounts the difference in the voltammogram. The capacity fading observed for different cycles (Fig. 1b) can also be explained by this partial irreversible nature of lithium-ion de-insertion in the monolayer after each cycle.

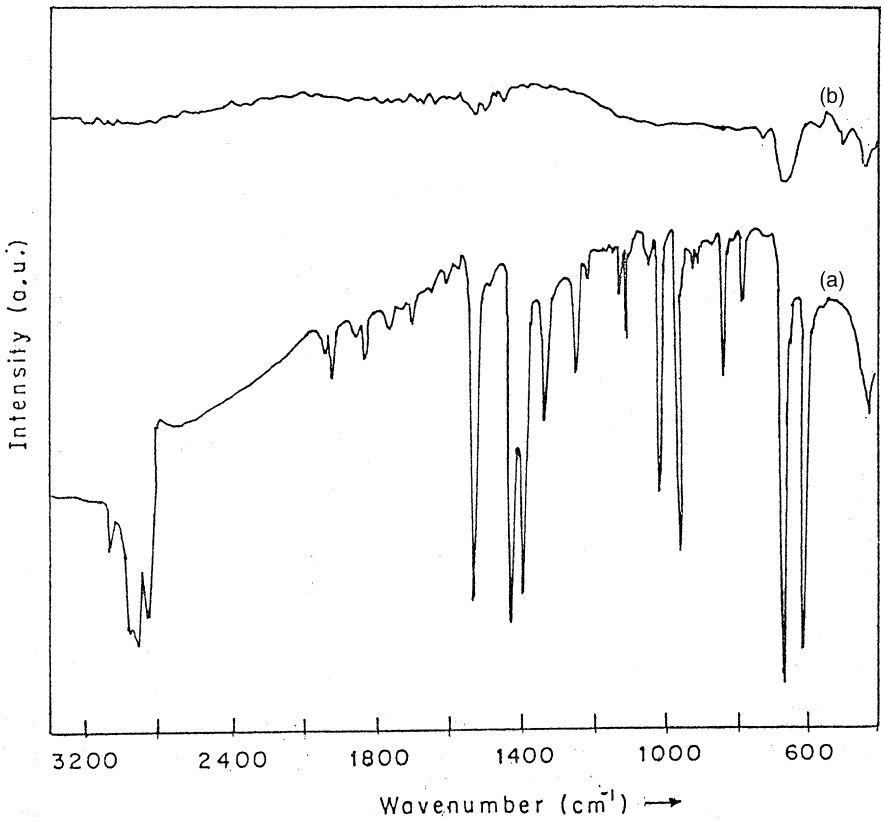

Fig. 5. FTIR spectra of (a) DDS powder and (b) DDS monolayer on Cu substrate; monolayer formed by immersing substrate in 1 mM DDS solution.

3.3. FTIR characterization

A comparison of the IR spectra of DDS powder and the DDS monolayer is given in Fig. 5(a) and (b), respectively. The spectrum for DDS powder was taken in order to confirm its purity and also for obtaining loss of distinct vibrational features after SAM formation. All the characteristic bands observed for DDS powder, such as C–H stretching (2850–2900 cm^{-1}), overtones or combinations (1600–2000 cm^{-1}), C–C ring stretching (1400–1600 cm^{-1}), out of plane C–C bending (688.5, and 736.8 cm^{-1}), C–S stretching (677 cm^{-1}) and S–S stretching (400–500 cm^{-1}) are in good agreement with the standard spectrum for pure DDS powder [29]. By comparison, Fig. 5(b) shows the absence of the S–S stretching band (400–500 cm^{-1}) after SAM formation. This indicates that the disulfide linkage has been cleaved, a conclusion that is in excellent agreement with QCM and scanning tunnelling microscopy (STM) investigations of DDS SAMs, where the facile S–S cleavage of DDS is inferred as one of the main reasons for the enhanced stability [28]. Further, the vibrational band seen as a shoulder around 677 cm^{-1} in the bulk DDS spectrum is shifted slightly to 678.9 cm^{-1} in the monolayer. This band can be attributed to the C–S stretching vibration and the shift suggests Cu–S bond formation [30]. Also, the bands between 350 and 450 cm^{-1} can be attributed to the stretching mode of Cu–S bond, which is formed subsequent to the disulfide cleavage during monolayer development [30]. Further, as the orientation of the aromatic ring changes after monolayer formation, the organization and tilt of molecules on a copper substrate, as well as the van der Waals interaction between adjacent molecules, may weaken the overtones and combination bands which correspond to the bezenethio group while all the remaining vibrational bands may become suppressed.

A comparison of the IR spectrum of discharged and charged samples is given in Fig. 6. Drastic changes can be seen in the spectral bands after charging and discharging as compared with the spectrum for the DDS SAM. For example in a discharged sample, the bands due to the overtones of the phenyl rings in the region 1600–2000 cm^{-1} are absent, while a pronounced new band appears at 1633.6 cm^{-1} (Fig. 6(a)). It is tentatively suggested that the appearance of this band (in both Fig. 6(a) and (b)) is due to π-cation interaction [31]. While, there is no direct evidence for the change in the relative orientation of phenyl rings with respect to each other in the SAM after lithium ion insertion/de-insertion, the disappearance of the aromatic overtone and combination bands suggests a change in the packing geometry of the phenyl ring planes. Also, the sharp peak appearing around 1087 cm^{-1} can be attributed to the stretching vibrations of the lithium salts, which are characterized by a broad continuum [32] at around 1250–1500 cm^{-1}. Similar variations are also observed in the IR spectrum of the charged sample

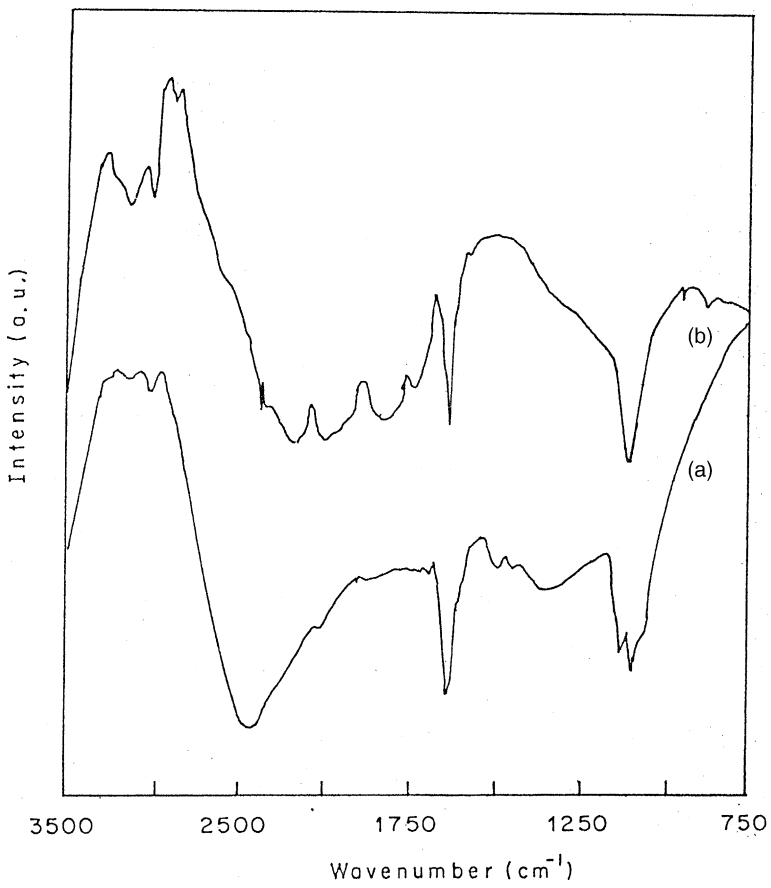

Fig. 6. FTIR spectra of (a) discharged DDS SAM and (b) charged DDS SAM; spectra recorded after removing samples from cell followed by thorough washing.

(Fig. 6(b)). Along with the dominant band at 1099 cm^{-1}, overtone bands are seen to reappear with a slight shift to higher frequency. This can be attributed to de-intercalation of lithium ions concomitant with rearrangement of the phenyl rings. A pronounced band at 1099 cm^{-1} for lithium salts still remains, however, with a shift to higher frequency giving support for quasi-irreversible Li^+ de-insertion, which can also explain the capacity degradation after a few cycles. These results are in good agreement with the cyclic voltammetric results for the charged sample which show both oxidation and reduction peaks (Fig. 4(b)) and where the appearance of the oxidation peak is attributed to partial irreversible de-intercalation of lithium ions.

3.4. X-ray photoelectron spectroscopy

XPS was used to monitor the changes that occur on the copper substrate and in the SAM before and after cycling. This analytical tool is used mainly because it can provide elemental composition (mainly lithium, sulfur and copper) and oxidation states of the elements present in the SAM. For all the samples, viz. DDS SAM, discharged SAM and charged SAM, the C 1s peak is symmetrical and can be Gaussian fitted with a single component. The binding energy profiles for Cu in SAM and discharged and a charged samples are shown in Fig. 7.

In all the cases, a shift in the binding energy of the Cu $2p_{3/2}$ and Cu $2p_{1/2}$ peaks to higher values (Table 1) along with pronounced shake-up features around 940 eV [24,33], which are characteristic of the Cu(II) oxidation state, is observed. This suggests partial oxidation of the copper substrate. A shift to higher values of the BE of Cu irrespective of charging or discharging indicates changes on the substrate due to oxide formation during cycling (Fig. 7(b) and (c)). This is expected since the insertion/de-insertion of Li^+ occurs primarily through interaction with the DDS monolayer.

Table 1
Binding energies of O 1s, Cu $2p_{3/2}$, Cu $2p_{1/2}$, S $2p_{3/2}$, Li 1s for DDS SAM, charged monolayer and discharged monolayer

BE values (eV)	O 1s	Cu $2p_{3/2}$	Cu $2p_{1/2}$	S $2p_{3/2}$	Li 1s
DDS SAM modified Cu	532.96	934.4	954.6	162.4	–
Charged SAM	533.4	937.4	957.4	164.2	52.4
Discharged SAM	532.4	935.2	955.6	163.4	51.4

After background correction the spectra have been fitted with Guassian curve.

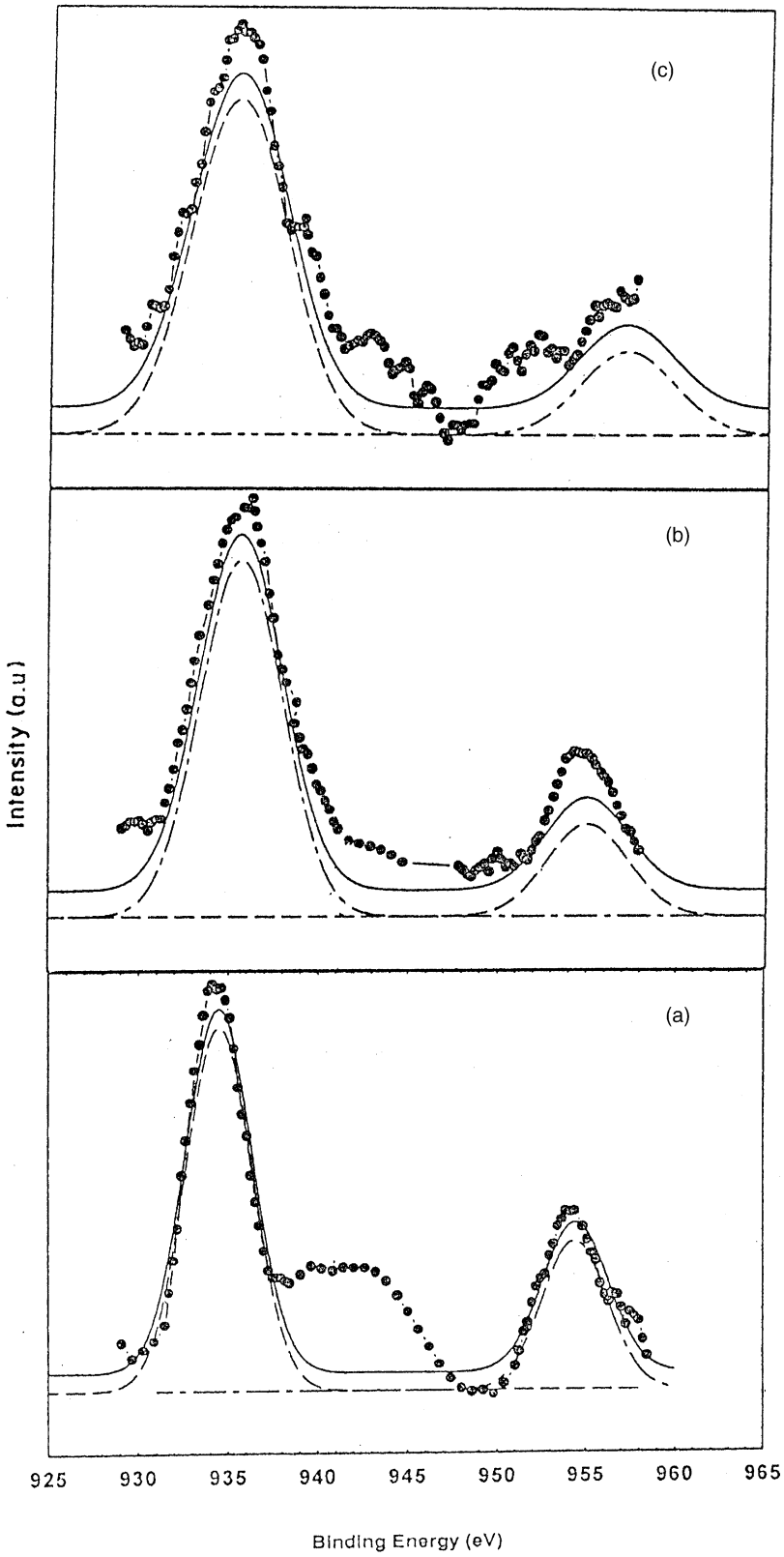

Fig. 7. Mg Kα induced XP spectra of Cu $2p_{3/2}$ and Cu $2p_{1/2}$ of (a) DDS monolayer, (b) discharged mono layer (c) charged monolayer, background correction spectra fitted with Guassian curve. Original data and component peaks are shown.

In comparison with the above results, the BE of sulfur should show interesting changes with respect to the charge–discharge process. For example, the S 2p XP signal, when fitted to the doublets of S $2p_{3/2}$ and S $p_{1/2}$ at 162.4 and 163.6 eV, shows decreasing and increasing BE values upon lithium ion insertion and de-insertion, respectively, compared with that for pristine SAM (162.4 eV). More specifically, the XP spectrum of the discharged sample gives S 2p at 163.4 eV (S $2_{p3/2}$) which differs from 164.04 eV (for standard S 2p). This shift corresponds to the adsorption of negative-charge bearing S on Cu metal. In a charged sample, the peak position shifts to a slightly to higher BE (164.2 eV). Clearly, these shifts are due neither to disulfonates nor oxidation products whose expected BE values are greater than 164.5 eV. Thus, the shifts can be indirectly co-related to the insertion and de-insertion of Li^+ ions on the monolayer. The additional peak at higher BE (168 eV) for all the samples is attributed to damage caused by the (sulfonate moiety) beam [33]. Also, the Li 1s peak obtained for the charged sample is shifted to a lower BE value (i.e. 55–51.4 eV) while a corresponding shift to a higher BE (52.78 eV) is observed for the discharged sample. This BE value for the charged sample can be explained by speculating that all the Li^+ ions are not de-intercalated during the charging process. This explanation is in agreement with the changes observed in the CV patterns presented in Fig. 4. Lastly, the enhanced intensity of the oxygen and lithium peaks for both charged and discharged samples indicates the formation of lithium compounds during cycling [34].

3.5. Mechanism of Li^+ ion insertion on DDS monolayers

To date, the nature of Li^+ ion interaction with SAM has not been sufficiently understood to elucidate a definite mechanism. On the basis of above experimental data, however, molecular models are proposed for the interactions of Li^+ (intercalation/de-intercalation) with the DDS monolayer. The first model is based on the simple assumption of lithium-ion interaction with the π-cloud of the benzene ring where the π-cation interaction is primarily responsible for Li^+ association (Scheme 1(a)). This can be supported from the IR spectrum of the discharged sample, where the overtones and combinations due to the benzene rings present in the pristine monolayer are missing. More interestingly, these bands do reappear in the spectrum for the charged sample where lithium-ion de-intercalation has taken place during charging. Thus, the reversible π-cation interaction is considered to be responsible for lithium-ion intercalation and cause orientational changes in the neighbouring benzene rings.

An alternate model based on the interaction of Li ions with the thiolate linkage can also be visualized (Scheme 1(b)) on the basis of the voltammetric results. Since the nature of the voltammogram obtained for both charged (quasi-reversible) and discharged (irreversible) electrodes is different, all the lithium ions intercalated are not able to de-intercalate and will thus result in the accumulation of some lithium ions in the monolayer. These Li ions are presumed to be irreversibly hooked up in the vicinity of Cu–S linkage and hence the thiolate bond is responsible for Li-ion association ($Li^{+\delta}$–$S^{-\delta}$).

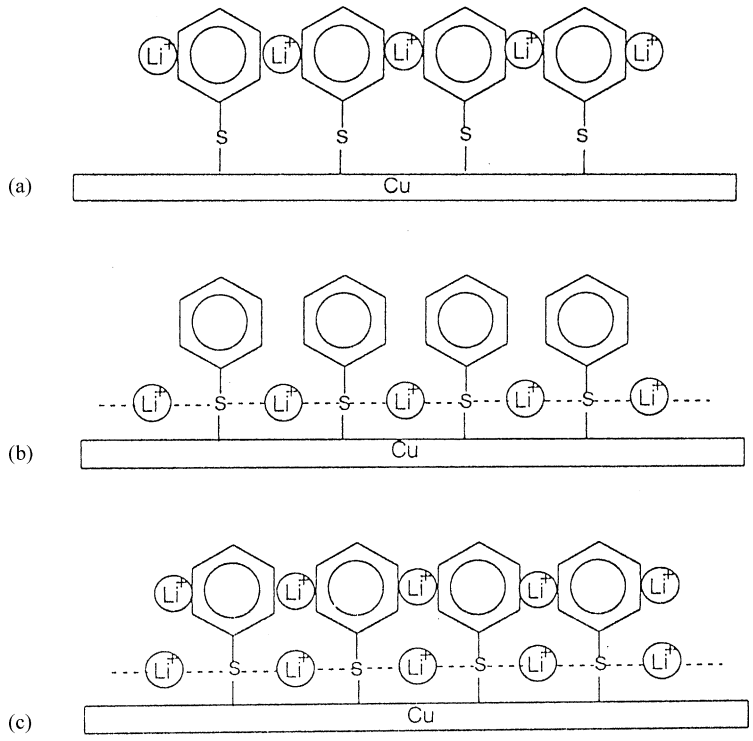

Scheme 1. Possible mechanism of Li^+ ion insertion on DDS monolayers based on: (a) π-cation interaction; (b) thiolate-lithium ion interaction; (c) combination of both interactions, π-cation and thiolate–lithium.

This is further supported by the fact that even bulk copper sulfide is a well-known cathode for non-aqueous lithium batteries [35].

Hence, multiple factors appear to contribute to Li^+ ion intercalation/de-intercalation on DDS SAM. It is also possible to consider a model which consists of both π-cation (responsible for the reversible behaviour) and thiolate-lithium ion (leading to irreversible nature) interactions, as shown in Scheme 1(c). Since the exact mechanism of the lithium-ion interaction with a monolayer cathode is not clear at the present, further studies using different substrates and thiol molecules are in progress.

4. Conclusions

The above results provide the first direct experimental evidence for the possibility of using self-assembled aromatic dithiol monolayers as cathode materials for rechargeable lithium batteries. This new class of nanostructured materials can electrochemically insert/de-insert lithium ions and facilitate high utilization. An especially striking feature is the high coulombic capacity in the initial cycles due to the quasi two-dimensional nature of the DDS monolayer. Infra-red and electrochemical measurements suggest orientational changes during the charge–discharge processes as a consequence of lithium-ion insertion. The findings clearly suggests a significant potential for SAMs as cathode materials for lithium batteries of high specific energy, provided capacity fading in the initial cycles can be alleviated by more robust SAM-forming molecules.

Acknowledgements

TM and MA are grateful to CSIR for the award of Senior Research Fellowships. KVJ thanks Ministry of Non-Conventional Energy Sources (MNES) for financial assistance.

References

[1] B. Scrosati, Nature 373 (1995) 557.
[2] N. Oyama, T. Tatsuma, T. Sato, T. Sotomura, Nature 373 (1995) 598.
[3] G. Pistoia, Lithium Batteries, Elsevier, Amersterdam, 1994.
[4] J. Desilvestro, J. Bass, Electrochem. Soc. 137 (1990) 50.
[5] T. Ohsuku, A. Ueda, J. Electrochem. Soc. 141 (1994) 2972.
[6] A. Yu, N. Kumagai, Z. Liu, J.Y. Lee, J. Power Sources 74 (1998) 117.
[7] M.E. Spahr, P. Stoshitzki-Bitterli, R. Nesper, O. Haas, P. Novak, J. Electrochem. Soc. 46 (1999) 146–2780.
[8] G. Ceder, Y.M. Chiang, D.R. Sadoway, M.K. Aydinol, Y.I. Jang, B. Huang, Nature 392 (1998) 694.
[9] J. Brodhead, F.A. TrumboraBasu, J. Electroanal. Chem. 118 (1981) 241.
[10] J. Kim, A. Manthiram, Nature 390 (1997) 265.
[11] M. Winter, J.O. Besenhard, M.E. Spahr, P. Novak, Adv. Mater. 10 (1998) 725.
[12] K. Mizushima, P.C. Jones, P.J. Wiseman, J.B. Goodenough, Mater. Res. Bull. 15 (1980) 783.
[13] T. Ohzuku, A. Ueda, T. Hirai, Chem. Exp. 7 (1992) 193.
[14] V. Manev, A. Momchilov, A. Kozawa, J. Power Sources 43–44 (1993) 551.
[15] (a) E. Peled, D. Golodnitsky, G. Ardel, J. Electrochem. Soc. 144 (1997) L208;
(b) M. Winter, P. Novak, A. Monnier, J. Electrochem. Soc. 145 (1998) 428.
[16] (a) W. Krawiec, L.G. Scanlon Jr., J.P. Fellner, R.A. Vaia, S. Vasudevan, E.P. Giannelis, J. Power Sources 54 (1995) 310;
(b) F. Leroux, B.E. Koene, L.F. Nazar, J. Electrochim. Soc. 143 (1996) L181;
(c) G.R. Goward, F. Leroux, L.F. Nazar, Electrochem. Acta. 43 (1998) 1307.
[17] M. Strattmann, Adv. Mater. 5 (1990) 191.
[18] R.C. Nuzzo, L.H. Dubois, D.L. Allara, J. Am. Chem. Soc. 112 (1990) 558.
[19] V. Depalma, N. Tiliman, Langmuir 5 (1989) 868.
[20] G.S. Ferguson, M.K. Chaudhury, G.B. Sigal, G.M. Whitesides, Science 253 (91991) 776.
[21] J. Chen, M.A. Reed, J.M. Tour, Science 286 (1990) 1550.
[22] H.E. Katz, W.L. Wilson, G. Scheller, J. Am. Chem. Soc. 116 (1994) 6636.
[23] J.J. Hickman, D. Ofer, D.E. Laibinis, G.M. Whitesides, Science 252 (1991) 688.
[24] H. Ron, H. Sophie Mathlis, M. Rappaport, I.J. Rubinstein, Phys. Chem. B. 102 (1998) 9861.
[25] K. Bandopadhyay, K. Vijaymohanan, Langmuir 15 (16) (1998) 5314.
[26] K. Bandopadhyay, M. Sastry, V. Paul, K. Vijayamohanan, Langmuir 13 (1997) 866.
[27] W.H. Li, R.J. Nichols, J. Electroanal. Chem. 456 (1998) 153.
[28] (a) M. Aslam, K. Bandopadhyay, K. Vijayamohanan, V. Lakshminarayanan, J. Colloid Interface Sci. 234 (2001) 410;
(b) K. Bandopadhyay, K. Vijayamohanan, M. Venkattaramanan, T. Pradeep, Langmuir 15 (1999) 5314.
[29] C.J. Pouchert, The Aldrich Library of Infra-Red Spectra, third ed., Aldrich Chemical Co. Inc., 1981.
[30] (a) C.J. Sandroff, D.R. Herschbach, J. Phys. Chem. 86 (1982) 3277;
(b) L. Raymond, M.A. Sobocinski, B. Jeanne, E. Pemberton, J. Am. Chem. Soc. 112 (1990) 6177.
[31] R.A. Kumpf, A. Dennis, S. Dougherty, Science 250 (1990) 1558.
[32] D. Aurbach, I. Weissman, Eectrochem. Commun. 1 (1999) 324.
[33] P.E. Laibinis, M.G. Whitesides, J. Am. Chem. Soc. 114 (1992) 9022.
[34] V.L. Colvin, A.N. Goldstein, A.V. Alivisatos, J. Am. Chem. Soc. 114 (1992) 5221.
[35] I. Fxnar, J. Hep, J. Power Sources 44 (1993) 701.